Magneto-optical study of interwell coupling in double quantum wells using diluted magnetic semiconductors

S. Lee, M. Dobrowolska, and J. K. Furdyna
Department of Physics, University of Notre Dame, Notre Dame, Indiana 46556

H. Luo
Department of Physics, State University of New York at Buffalo, New York 14260

L. R. Ram-Mohan
Departments of Physics and Electrical and Computer Engineering, Worcester Polytechnic Institute, Worcester, Massachusetts 01609
(Received 10 July 1996)

Magneto-optical experiments were carried out on a series of $ZnSe/Zn_{1-y}Cd_ySe$ double quantum wells coupled by $Zn_{1-x}Mn_xSe$ diluted magnetic semiconductor (DMS) barriers. The samples consisted of 45-Å nonmagnetic quantum wells with interwell DMS barriers of different thicknesses (10, 35, and 100 Å). The interband ground-state transition, as well as interband transitions between excited states, were observed. As the magnetic field is applied, the heights of the magnetic barriers in the conduction and in the valence band undergo Zeeman shifts, causing major changes in the interwell coupling. Such changes were studied by examining the energies of the transitions, their Zeeman splittings, and their intensities. The dependence of these effects was further studied as a function of temperature and barrier width. The behavior observed in those cases involving ultrathin magnetic barriers was found to be anomalous, and is discussed in terms of effects of reduced dimensionality on the magnetic properties of thin DMS layers. [S0163-1829(96)07848-4]

I. INTRODUCTION

Diluted magnetic semiconductors (DMS's) are semiconducting alloys in which a part of the semiconductor crystal lattice is substitutionally replaced by magnetic transition-metal ions. II-VI semiconductors in which a fraction of the group-II atoms is replaced by Mn^{2+} are the best-known examples of such alloys (e.g., $Zn_{1-x}Mn_xSe$). One of the remarkable properties of these materials is that they exhibit an extremely large Zeeman splitting of the band edges due to exchange interaction between the *d* electrons of Mn^{2+} and the band electrons.[1] This has special implications for semiconductor heterostructures, such as quantum wells (QW's) and superlattices (SL's) made up of DMS and non-DMS layers, because we can use the large Zeeman splitting in such structures to vary the relative band alignment in the adjacent layers simply by applying a magnetic field. This then provides a unique opportunity to investigate the effect of band alignment on the properties of a given heterostructure in a continuous manner.[2]

One of the most interesting semiconductor heterostructures is the double quantum well (DQW) geometry, comprised of two quantum wells separated by a thin barrier layer. Interwell interaction (i.e., coupling) is then an extremely sensitive function of the barrier separating the wells. Clearly, the thinner or the lower the barrier, the greater the interaction between the wells. As a result of this interaction, each state occurring in an isolated single QW will now split into a symmetric and an antisymmetric state, the two states having different energies. The splitting of the energy levels due to the coupling between the two wells is of course mainly determined by the barrier.[3]

Molecular beam epitaxy (MBE) allows us to fabricate DQW's with various barrier widths or heights, the latter achieved by adjusting the composition of the alloy used as the barrier material. Furthermore, if the barrier is made from a DMS alloy, the giant Zeeman splitting in DMS's already mentioned will allow us to tune the barrier height continuously during the experiment by an external magnetic field. The DQW's coupled by thin DMS layers then provide a unique laboratory for investigating the effect of the barrier potential on interwell coupling, and it is especially important that this can be done continuously in a single sample.

Figure 1 shows a typical DQW structure investigated in this study. The quantum wells consist of 45-Å nonmagnetic $Zn_{1-y}Cd_ySe$ layers ($y \approx 0.2$); each DQW pair is bordered on the left and right by thick ZnSe layers; and the barriers separating the wells within each DQW pair are magnetic $Zn_{1-x}Mn_xSe$ ($x \approx 0.2$) layers. The degeneracy of the valence band is removed by the joint effect of confinement energy of the wells, and of uniaxial strain[4] arising from the lattice mismatch between $Zn_{1-y}Cd_ySe$ wells and the ZnSe outer barriers. When the strain is compressive (as it is in the present case), both effects are additive, shifting the light holes far below the top of the heavy-hole valence band. In this paper we will not be concerned with light-hole transitions: they are weak, and their Zeeman shift (the focus of our investigation) is at least an order of magnitude smaller than that of heavy-hole transitions. Thus, only heavy-hole bands are depicted in Fig. 1. Earlier investigations of such structures were carried out by magnetophotoluminescence,[5] which provides information only on the spin-down component of the symmetric ground state of the DQW, to which all other states relax before recombination. In this paper we are interested in interwell *coupling* in the DQW structure, and thus in the *splitting* between the symmetric and the (higher-lying) antisym-

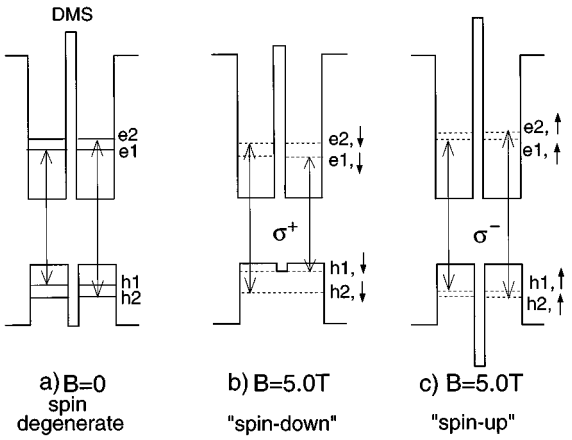

FIG. 1. Band alignment of a double quantum well coupled by a DMS barrier, showing two lowest eigenstates in the conduction and valence bands. The states are spin degenerate for $B=0$ (a). When a magnetic field is applied, the spin-down states (b) and spin-up states (c) shift differently, because each spin orientation ''sees'' a different barrier (lower for spin down, higher for spin up). Vertical arrows show the allowed optical transitions.

metric states. Magnetoabsorption, which provides information on transitions involving both symmetric and antisymmetric states, and on their magnetic field dependence, is thus ideally suited for investigating interwell coupling in a DQW, and its relation to barrier parameters.

The magnetoabsorption experiments were carried out in the Faraday geometry, i.e., with magnetic field applied perpendicular to the layer planes of the DQW structures, and with light incident normally on the sample. In this geometry the spin-down and the spin-up states ''see'' different barrier heights when the field is applied, as determined by the Zeeman splitting of the band edges in the DMS material. Since—as discussed in the following section—the heavy-hole band has a much stronger exchange interaction (about four times) than the conduction band, and a relatively small band offset, we expect particularly strong variations of the interwell coupling in the heavy-hole band, as illustrated schematically in Figs. 1(b) and 1(c).

In this geometry, we studied a series of symmetric DQW's with DMS barriers of different thicknesses (see Table I), which determine the initial (i.e., $B=0$) degree of coupling. Then, by applying a magnetic field, we were able to follow in a continuous manner the variation of the coupling as the Zeeman-induced barrier height was changing.

II. THE MECHANISM OF ZEEMAN SPLITTING IN DMS's

Since the Zeeman splitting of band edges in the DMS layers is of central importance in this investigation, we briefly discuss the mechanism of this phenomenon before proceeding further. The effect arises from the spin-spin exchange interaction referred to earlier. The Hamiltonian describing the exchange interaction[1] in DMS's is given by

$$H_{\mathrm{ex}}=\sum_i J^{sp\text{-}d}(\mathbf{r}-\mathbf{R}_i)\mathbf{S}_i\cdot\boldsymbol{\sigma}, \tag{1}$$

where $J^{sp\text{-}d}$ stands for the sp-d exchange integral between the band electrons and the Mn^{2+} ions; $\mathbf{r}$ and $\mathbf{R}_i$ are the positions of band electrons and of the Mn^{2+} ions, respectively; and $\boldsymbol{\sigma}$ and $\mathbf{S}_i$ are the spin operators for the band electron and for the Mn^{2+} ion, respectively. Using the mean field and the virtual crystal approximations, this Hamiltonian can be cast in a form that has the periodicity of the crystal lattice,[1] and can thus be incorporated into the total Hamiltonian of the host semiconductor. To analyze the band structure of a semiconductor in the presence of a magnetic field, one often uses the powerful eight-band model.[6,7] Using H_{ex} in this model, one obtains the shift of the conduction and valence bands relative to their zero-field values (the Zeeman shift) as

$$\Delta E_c=\alpha N_0\overline{x}\langle S_z\rangle, \tag{2}$$

$$\Delta E_v=-\beta N_0\overline{x}\langle S_z\rangle, \tag{3}$$

where N_0 is the number of cations per unit volume, α and β are sp-d exchange integrals for the conduction and the valence bands, respectively, $\overline{x}$ is the *effective* Mn^{2+} concentration, and $\langle S_z\rangle$ is the average spin per Mn^{2+} ion. For $Zn_{1-x}Mn_xSe$, of interest here, $\alpha N_0=0.29$ eV and $\beta N_0=-0.88$ eV (Ref. 2). The physical interpretation of $\overline{x}$ and $\langle S_z\rangle$ is discussed below.

Consider a DMS alloy (e.g., $Zn_{1-x}Mn_xSe$) with an atomic fraction x of Mn^{2+} ions. At very low concentration (in the limit of noninteracting magnetic moments, say, $x<0.005$), all x Mn^{2+} ions contribute to the total magnetic moment, with the average spin per magnetic ions, $\langle S_z\rangle$, described by the Brillouin function. As x increases, the antiferromagnetic interaction between Mn^{2+} ions reduces the number of ions contributing to the total spin. For example, spins of nearest-neighbor Mn^{2+} pairs cancel out. We then resort to an empirical parameter $\overline{x}$, which is an *effective* concentration of those Mn^{2+} ions contributing to the total magnetic moment. This parameter is of special significance in the present paper (in connection with our discussion of ultrathin barriers and the effects of reduced dimensionality), and we discuss it here for future convenience. It is easy to see that $\overline{x}\to 0$ as $x\to 0$, but also that $\overline{x}\to 0$ as $x\to 1$, where all Mn^{2+} spins cancel one another. Thus $\overline{x}$ is always less than x (the difference becoming greater with increasing x), and must display a maximum value at some intermediate Mn^{2+} concentration.

TABLE I. Sample description.

Sample	Well	Barrier	L_w	L_b	y	x
1	$Zn_{1-y}Cd_ySe$	$Zn_{1-x}Mn_xSe$	45 Å	10 Å	0.20	0.20
2	$Zn_{1-y}Cd_ySe$	$Zn_{1-x}Mn_xSe$	45 Å	35 Å	0.19	0.20
3	$Zn_{1-y}Cd_ySe$	$Zn_{1-x}Mn_xSe$	45 Å	100 Å	0.25	0.20

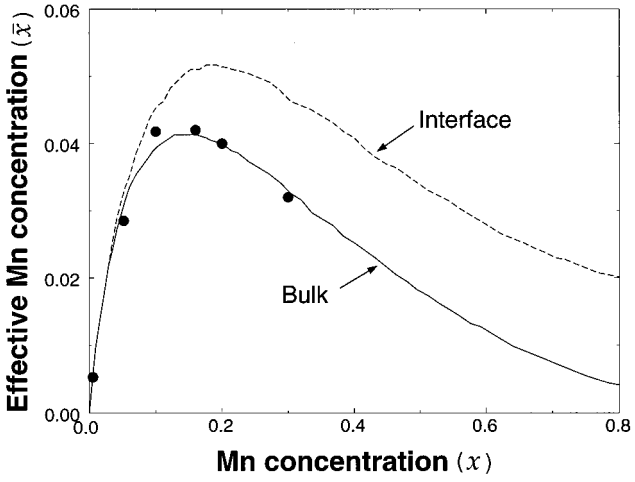

FIG. 2. The relation between x and $\overline{x}$ in bulk DMS's and at the DMS/non-DMS interface, shown as a solid and a dotted line, respectively, as given in Ref. 8. The enhancement of paramagnetism at the interface is clear over the region $x \geqslant 0.1$. The solid dots correspond to experimental values obtained on a series of $Zn_{1-x}Mn_xSe$ epilayers, including the ''companion'' epilayer used in this investigation.

The relation between the effective concentration parameter $\overline{x}$ and the actual (i.e., chemical) concentration x of Mn^{2+} over the range $0 \leqslant x \leqslant 0.8$ has been investigated by Fatah *et al.*[8] The authors performed numerical simulations of the antiferromagnetic spin pairing of neighboring magnetic ions. The plot of $\overline{x}$ as a function of x in Fig. 2 (solid line) shows the results of the simulation that includes only nearest-neighbor pairing. We also show in the figure, as full points, the values of $\overline{x}$ and x, which we measured on a series of $Zn_{1-x}Mn_xSe$ epilayers, including the ''companion'' epilayer, which was used to calibrate the barrier layers in the present study. The agreement between the calculated and experimental values of $\overline{x}$ is excellent, implying that at low fields only those spins that do not have antiferromagnetically paired nearest neighbors are able to contribute to the magneto-optical response of the system. (We will return to the dashed curve in Fig. 2 in Sec. V C.)

The parameter $\langle S_z \rangle$ is then the thermal average of the spin of the contributing ions (such that $\overline{x}\langle S_z \rangle$ is the total spin per unit volume of the alloy). While it is a phenomenological parameter, it can (in analogy with the ultradilute case of noninteracting spins) be expressed by a *modified* Brillouin function $B_{5/2}$, as follows:

$$\langle S_z \rangle = \frac{5}{2} B_{5/2}\left[\frac{\frac{5}{2} g \mu_B B}{k_B (T + T_0)}\right]. \tag{4}$$

In the argument of $B_{5/2}$, above, g is the Landé g factor of Mn^{2+} ($g = 2$), μ_B is the Bohr magneton, B is the external magnetic field, k_B is the Boltzmann constant, T is the temperature, and T_0 is a phenomenological parameter that takes into account the antiferromagnetic interaction among unpaired (''loose'') spins. It represents the ability of these ''loose'' spins to align under the influence of an external magnetic field.

In DQW's involving DMS interwell barriers, such as those used in the present study, changes in coupling induced by the magnetic field are extremely sensitive to the magnetic properties of those barriers. Since the barrier layers are thin, this situation provides a unique opportunity to investigate the magnetism of thin DMS layers. In particular, because thin layers are characterized by a high interface-to-volume ratio, this situation provides an excellent opportunity for investigating the contribution of the interface to the magnetic properties of the layered structure, as discussed at the end of Sec. V.

III. EXPERIMENTS

$ZnSe/Zn_{1-y}Cd_ySe$ DQW's coupled by $Zn_{1-x}Mn_xSe$ barriers were grown by MBE on 2-μm ZnSe buffer layers, deposited directly on GaAs (100) substrates. The DMS barrier thicknesses in the three DQW's were 10, 35, and 100 Å, respectively, and the well width was kept the same ($L_w = 45$ Å) in all three samples. In order to determine the concentration x (and thus the magnetic properties) of the $Zn_{1-x}Mn_xSe$ barrier layer, ''companion'' $Zn_{1-x}Mn_xSe$ epilayers were prepared under the same MBE growth conditions as those used in growing the interwell DMS barriers.

For transmission experiments, the GaAs substrate was removed from the sample by mechanical polishing, followed by suitable chemical etching (1:20 $NH_4OH : H_2O_2$ at room temperature). The absorption experiments were performed in an optical cryostat ($T \geqslant 1.5$ K) equipped with a 6-T superconducting magnet. The light source used in the experiments was a halogen lamp with a 1-m monochromator. The monochromatic light was circularly polarized, so as to allow the identification of transitions between different spin states. The signal was detected by a photomultiplier tube, and was sent to a lock-in amplifier and a computer-controlled analyzer for data storing and processing.

IV. RESULTS: QUALITATIVE DESCRIPTION

A. Identification and energies of transitions

Absorption spectra for the DQW with a 10-Å magnetic barrier are shown in Fig. 3 for several magnetic fields, for both σ^+ and σ^- circular polarizations. In the absence of a magnetic field three excitonic peaks are observed. The two stronger absorption peaks, at 2.600 and 2.629 eV, are identified as the heavy-hole exciton transitions from the lowest symmetric (e_1h_1) and antisymmetric (e_2h_2) states, respectively. These identifications are made on the basis of the behavior of these absorption peaks after the magnetic field is applied (marked by the thin dashed line) since, as was already mentioned, the heavy-hole excitons shift much more rapidly than the light-hole excitons as the field increases. In this sample the barrier is thin, so that the interaction between the wells is strong, and consequently the distance between the (e_1h_1) and (e_2h_2) peaks is quite large.

The third weak and wide peak at 2.662 eV is attributed to the light-hole exciton. (Although weak on the scale of the figure, the peak is quite unambiguous when detected at higher sensitivity.) As mentioned earlier, the $Zn_{1-y}Cd_ySe$ wells in our samples are under compressive strain imposed by the ZnSe outer barriers, which, together with confinement

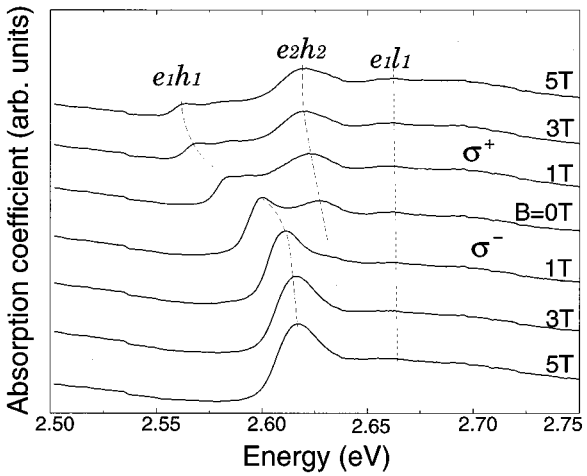

FIG. 3. Absorption spectra for a DQW with a 10-Å barrier at different magnetic fields. σ^+ and σ^- refer to spin-down and spin-up transitions, respectively.

effect of the wells, pushes the light-hole band up to higher energies, thus resulting in a very small band offset and weak carrier localization for the light-hole band. Consequently, the light-hole excitonic peaks are weak and wide. In this paper we will not be interested in the light-hole transitions, except to use the splitting between the heavy- and the light-hole exciton peaks for determining the amount of strain[9] in the system, which is then used in the calculations. The light-hole band is also automatically included when we calculate heavy-hole eigenstates in DWQ's by using the eight-band model in the presence of the magnetic field, as discussed in Sec. V A.

The magnetic field dependence exhibited by the other DQW's used in this study is qualitatively similar to that shown in Fig. 3. Figure 4 is a summary plot, showing the observed transition energies for each polarization as a function of magnetic field, for all samples. The transitions related to the symmetric and the antisymmetric states (i.e., e_1h_1 and e_2h_2) in the sample with the thinnest barrier (10 Å) are clearly seen in zero magnetic field, separated by over 29 meV. Although e_2h_2 is too weak to be observed at $B=0$ in the DQW with a 35-Å barrier, extrapolation from high-field σ^+ transitions indicates the zero-field splitting to be only 16 meV for that sample, indicating much weaker coupling, as would be expected for a thicker barrier. In the sample with the 100-Å barrier the two peaks are not even resolved. Thus, as expected, the thinner the barrier, the stronger the interwell coupling, and the bigger the splitting between the e_1h_1 and e_2h_2 transition energies.

The energy levels of each state of the DQW are spin degenerate at zero magnetic field. When the magnetic field is applied, however, barrier heights in both the conduction and the valence bands decrease for spin-down states, and increase for spin-up states. As a result, transitions associated with the spin-down states (those seen with σ^+ polarization of light) move further apart (stronger coupling), and those involving spin-up states (seen in σ^- polarization) move closer together. As seen in Figs. 3 and 4, the antisymmetric state transitions (e_2h_2) show a significantly smaller shift compared to that of the symmetric state transitions, as the

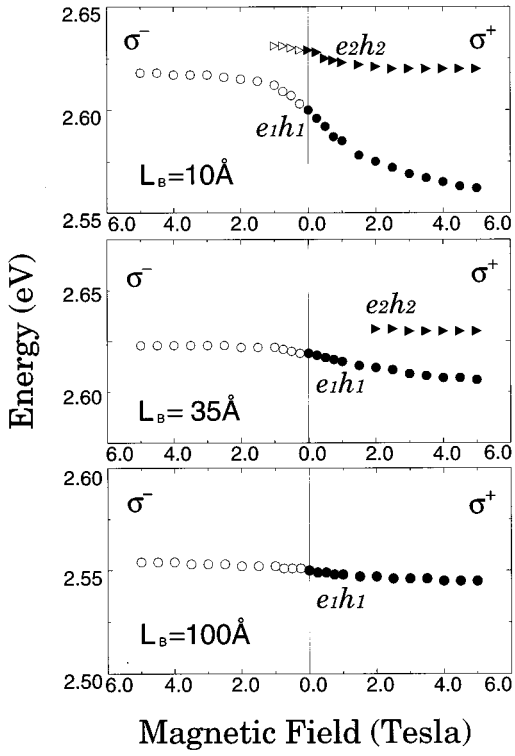

FIG. 4. Transition energies for the e_1h_1 and e_2h_2 transitions observed in σ^+ and σ^- circular polarizations, plotted vs magnetic field for DQW's with 10-, 35-, and 100-Å DMS barriers. The σ^+ data are designated by solid symbols, σ^- by open symbols. The e_1h_1 transition energy for the 100-Å barrier is lower than for the two other structures because of the slightly larger Cd content in the wells (see Table I).

barrier height changes with magnetic field. This is because the probability density $|\Psi|^2$ (where Ψ is the wave function) for the antisymmetric states has a node at the center of the DMS barrier, and is thus much less sensitive to the barrier height than the symmetric states. This effect of the probability distribution with respect to the barrier will be discussed in considerable detail later in the paper.

A particularly important feature of this experiment is the ability to continuously change the interwell coupling with the magnetic field. For example, in the sample with the thinnest barriers (10 Å), which shows excitonic transitions from both the symmetric and the antisymmetric states at $B=0$, we can clearly follow the change in the interwell coupling as the barrier heights of the DQW are varied by the applied magnetic field. Since the energy separation between the two transitions is a direct indication of the coupling strength, it is clear that the coupling between the wells is increased for the spin-down (σ^+) transitions, and is decreased for the spin-up (σ^-) transitions. This continuous change of interwell coupling as a function of the applied magnetic field is quite obvious in Fig. 4. We wish to call attention to the range of tunability of the e_1h_1 level made possible by varying the barriers. This is particularly evident in the case of the sample with the thinnest barrier, where it reaches about 40 meV, more than half of the zero-field heavy-hole band offset, and almost as much as the total Zeeman shift exhibited by the companion epilayer, as shown in Fig. 5.

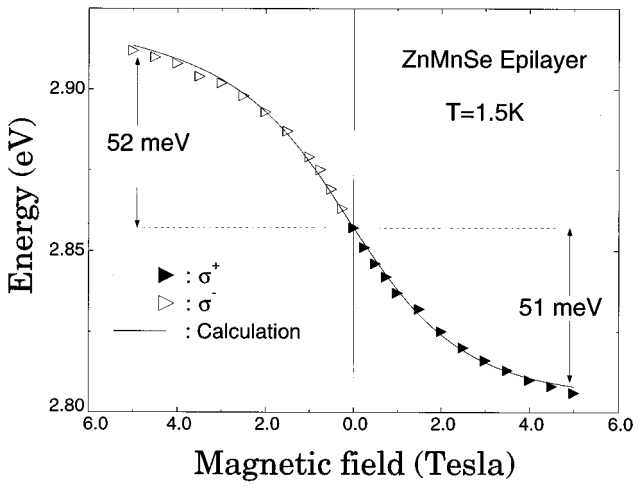

FIG. 5. Transition energies of the companion $Zn_{1-x}Mn_xSe$ epilayer for σ^+ and σ^- polarizations. Triangles are experimental. The solid line is calculated using the effective Mn^{2+} concentration of $\overline{x}=0.04$ and $T_0=2.95$ K.

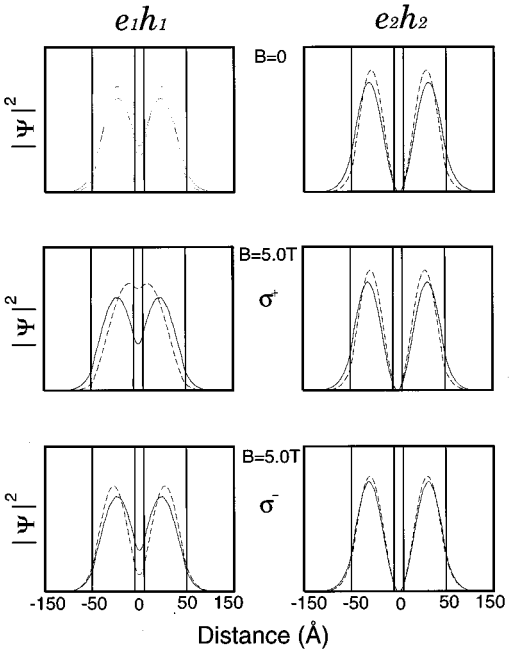

FIG. 6. The square of the electron and hole wave functions for the lowest two spin-down and spin-up states, calculated for the DQW with a 10-Å DMS barrier for $B=0$ and 5 T. The solid and dashed lines represent electrons and holes, respectively. Clearly, the h_1 spin-down state tunnels more easily through the magnetic barrier, presenting a large probability density at the barrier. The wave functions were calculated using the eight-band model, as described in Sec. V.

As the thicknesses of the barriers increase, interactions between the wells become weaker, and the observable variations of interwell coupling become correspondingly smaller. In the sample with the 35-Å barrier we are still able to observe a clear splitting between the two lowest spin-down transitions as the magnetic field is applied. However, we have not observed the splitting of these transitions in the sample with the thickest (100 Å) barriers. This is not surprising, since with such a large value of L_b this DQW sample behaves in effect like two uncoupled single QW's, and the magnetic field does not alter this situation.

B. Transition intensities

In the absorption spectra observed for the DQW's, the e_1h_1 transitions for the σ^+ polarization are systematically weaker than those for σ^-, the intensity ratio (σ^+/σ^-) decreasing with increasing magnetic field. This might be expected from the wave-function overlap for electron and hole states involved in the transition. The probability distributions for the two lowest electron and hole subbands are shown in Fig. 6, where $|\Psi|^2$ for electrons and for holes is indicated, respectively, by solid and dashed curves, and the vertical lines define the $ZnSe/Zn_{1-y}Cd_ySe$ and $Zn_{1-y}Cd_ySe/Zn_{1-x}Mn_xSe$ interfaces. (The wave functions used to generate the figure were calculated using the eight-band model described in Sec. V, with parameters corresponding to a DQW with a 10-Å barrier at 1.5 K.)

At zero magnetic field, both carriers are mostly localized in the $Zn_{1-y}Cd_ySe$ wells due to the large confinement potential. When a magnetic field is applied, most of the potential variation in the barrier region occurs in the heavy-hole band, while the conduction-band barriers experience relatively little change (see Fig. 1). Consequently, the magnetic field has relatively little effect on the electron states, and their probability distribution remains almost the same as at zero magnetic field. It should also be noted that the antisymmetric states for holes show very little change of the wave function (even though the shift of the heavy-hole band edge at 5 T is comparable to the heavy-hole band offset) due to the fact that these states have zero probability density at the center of the barrier. The only noticeable wave-function change is thus in the symmetric heavy hole states, which have a sizable probability density in the magnetic barrier. This is very clear, for example, for the spin-down hole states (middle left panel), which strongly penetrate the center barrier, and are thus highly sensitive to the barrier height. Since the variations of the conduction- and valence-band edges are in this case very different, the electron-hole wave function overlap for spin-down states is significantly reduced, and the e_1h_1 absorption intensity is thus expected to decrease with field for the σ^+ polarization.

Furthermore, it is well known that the optical absorption intensity in a heterostructure depends not only on the wave-function overlap, but on carrier localization as well. In single quantum wells (SQW's) the absorption intensity monotonically decreases as the well width increases in the range $L_w > a_B$ (where a_B is the exciton Bohr radius), since increasing the well width reduces the carrier localization.[10] In ZnSe/$Zn_{1-x}Mn_xSe$ systems, the exciton Bohr radius is approximately 35 Å. In DQW's consisting of 45-Å wells, the carrier confinement may change as the height of the central barrier changes with magnetic field. Specifically, for the heavy-hole spin-down states, the central barrier height is lowered quite dramatically with increasing magnetic field, and the entire structure eventually approaches a *single quantum well* with more than twice the original well width. It is reasonable to expect that the carrier confinement continuously decreases in this situation (as it would with increasing well thickness in a

SQW), causing the absorption intensity to drop. As a result of both effects (reduction in overlap and reduction in localization), the e_1h_1 absorption intensity for σ^+ polarization is therefore expected to fall with increasing magnetic field, as is clearly observed experimentally (see Fig. 3).

The intensity of transitions involving antisymmetric states also changes as the magnetic field is varied. But this behavior cannot be explained by the wave-function overlap for the electron and hole states, since the antisymmetric state wavefunctions remain essentially unchanged for both carriers. However, we note that the e_2h_2 transitions become stronger just when the e_1h_1 transitions become weaker, and vice versa, the total intensity of these transitions remaining approximately constant. This strong correlation between intensities of the two transitions as the coupling is varied suggests some sort of sum rule that governs both transitions together. We argue this as follows.

In general, optical transitions in heterostructures will have stronger absorption intensity when the same structures are repeated. An obvious example is the case of two individual single QW's separated by a barrier of large height or width. In such a structure transitions are expected to be twice as strong as in a single QW, since the states involved now have exactly the same energy, and twice the oscillator strength. In DQW's studied here, two SQW's are repeated with a small barrier thickness, and the ground states do not exactly overlap, but are split into two states (symmetric and antisymmetric) due to the interaction between the wells. However, these two states *originate* from the same ground state of the constituent SQWs, before they become coupled to each other. Thus, the *cumulative* intensity of these (e_1h_1 and e_2h_2) transitions would be expected to be the same as that of the ground-state transitions in two uncoupled SQW's. In this picture, the total intensity should not depend on the coupling strength between the wells. The experimentally observed behavior shown in Fig. 7 (where the sum of the two intensities remains roughly constant as the interwell coupling is varied by the magnetic field) appears to confirm this interpretation. Thus, if we impose the condition that the total intensity of e_1h_1 and e_2h_2 transitions should remain constant, together with the observed variation of e_1h_1 (which we can understand on the grounds of wave-function overlap and localization), we must *require* that the intensity of e_2h_2 transitions increases as e_1h_1 decreases, and vice versa. This behavior is quite clear in both samples with thin barriers (two upper panels in Fig. 7), and is further corroborated by the constant absorption intensity observed for the widest (100 Å) barrier, where the two wells are essentially uncoupled at all fields (lowest panel).

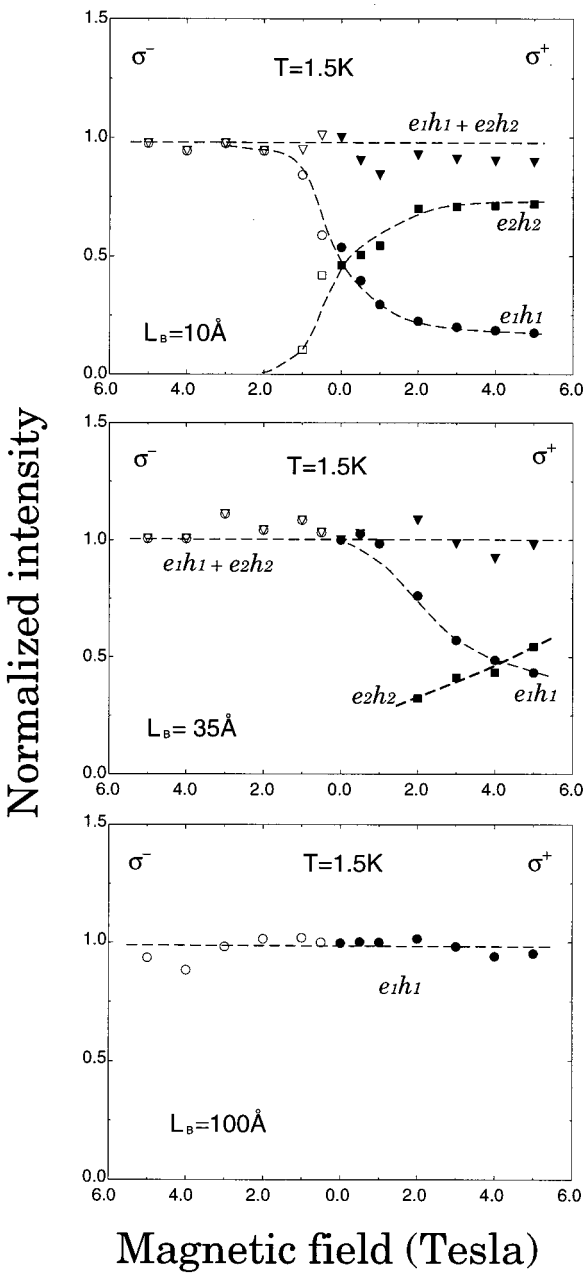

FIG. 7. Intensities for the symmetric (circles) and antisymmetric (squares) transitions, and the sum of both transitions (triangles), plotted vs magnetic field for the σ^+ (full symbols) and σ^- (open symbols) circular polarizations for DQW's with L_b = 10, 35, and 100 Å. Intensities are normalized to the total intensity at zero field. The dashed lines are guides for the eyes.

C. Temperature dependence

In general, the Zeeman splittings of the band edges in the DMS's show a dramatic decrease with increasing temperature due to the thermal fluctuation of Mn^{2+} spins. In the case of the DQW studied here, the magnetic-field-induced variation of the DMS barrier height will thus also depend on the temperature, and this will be reflected in the degree of interwell coupling. Figure 8 compares the magnetic field dependence of the e_1h_1 and e_2h_2 transitions in the DQW with a 10-Å DMS barrier observed at 1.5 and 30 K. As expected, the observed shifts of both lines are significantly smaller at 30 K, but parallel the low-temperature behavior in that the magnetic-field-induced shift for e_2h_2 is much smaller than the e_1h_1 shift. Thus the coupling (as measured by the separation of these two transitions) is weaker at 30 K for the spin-down states, but stronger for the spin-up states, than it was at 1.5 K.

We have noted in Sec. IV B that the e_2h_2 transition loses its intensity with decreasing coupling. Thus at 1.5 K it vanished for the spin-up transitions at fields above 1 T (see open

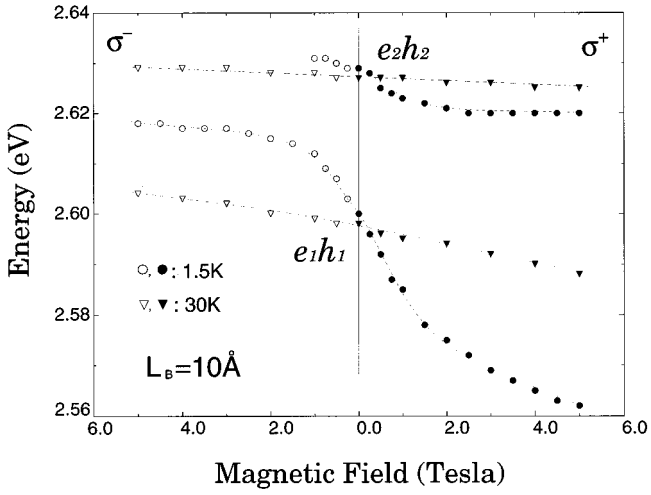

FIG. 8. Transition energies for the DQW with a 10-Å barrier at 10 and 30 K, plotted as a function of magnetic field. The dotted lines are a guide for the eyes.

circles in Fig. 8), due to the increasing barrier height as seen by the σ^- polarization. At 30 K the barrier height in the σ^- polarization increases much more slowly with field, so that the coupling between the spin-up states is stronger at any given field (as already observed in connection with Fig. 8). This in turn leads to the surprising result that the intensities of the spin-up e_2h_2 transitions actually *increase* with increasing temperature at high field, and can be seen throughout the entire field range at this temperature (open triangles in Fig. 9). This enables us to investigate the relationship of the e_1h_1 and e_2h_2 intensities over the whole range of fields available, as shown in Fig. 9. The 30-K data very nicely corroborate the ''sum-rule'' discussion for these two transitions, given above. Since exciton transitions generally become weaker with increasing temperature, the fact that the spin-up e_2h_2 line actually intensifies at 30 K (it is

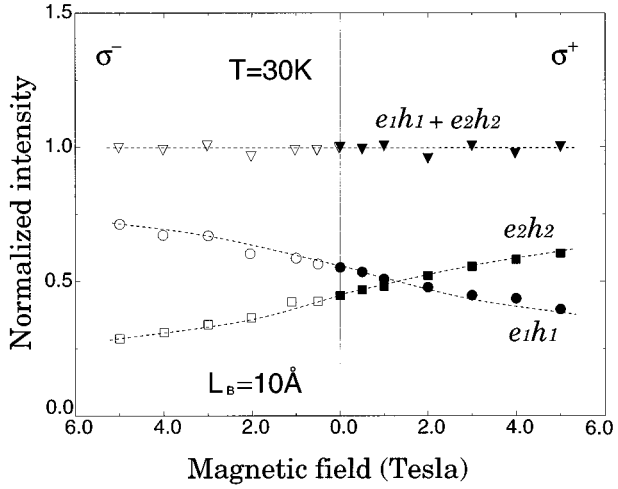

FIG. 9. Intensities for the symmetric and antisymmetric transitions, and their sum, plotted as a function of magnetic field for the σ^+ and σ^- circular polarizations, observed at 30 K for the DQW with $L_b = 10$ Å. Intensities are normalized to total intensity at zero field. Dashed lines are guides for the eyes.

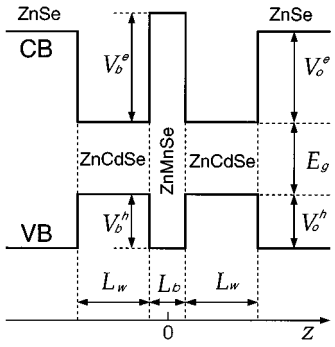

FIG. 10. Schematic view of the potential profile for a DQW. L_w and L_b are the respective layer thicknesses for the well and the DMS barrier. $V_o^{e,h}$ and $V_b^{e,h}$ denote the outside and the central barrier potentials for electrons and holes. CB and VB indicate the conduction- and the valence-band edges, respectively, and E_g is the energy gap of the $Zn_{1-x}Cd_xSe$ well material.

not even observable at 1.5 K) adds additional strength to the argument that the intensities of the e_1h_1 and e_2h_2 are somehow jointly determined by the coupling of the states involved in these transitions.

V. RESULTS: QUANTITATIVE ANALYSIS

A. Theoretical model

In heterostructures comprised of different semiconductors, the misalignment of conduction and valence bands at the interfaces (the so-called ''band offset'') results in square well and barrier potentials. The behavior of carriers in such heterostructures (e.g., the DQW) can be described by using the ''envelope function approximation,''[11,12] as discussed below.

In a bulk semiconductor crystal, the wave function can be expressed as

$$\psi_{n,\vec{k}}(\vec{r}) = e^{i\vec{k}\cdot\vec{r}} u_{n,\vec{k}}(\vec{r}), \tag{5}$$

where $u_{n,\vec{k}}(\vec{r})$ is the periodic Bloch function, and n is the band index. Because of the lack of infinite translational symmetry along the growth direction, the wave function describing the heterostructure can be written as

$$\psi_{n,\vec{k}}(\vec{r}) = e^{ik_x x} e^{ik_y y} f_{k_z}(z) u_{n,\vec{k}}(\vec{r}). \tag{6}$$

Now the wave function consists of the Bloch functions (which vary on a scale of the unit cell of the bulk crystal) and the envelope function f_{k_z} (which varies on the scale of heterostructure layers). By applying effective mass theory,[13] this wave function leads to the following Schrödinger equation for the envelope function:

$$Hf(z) = \left[-\frac{\hbar^2}{2m^*(z)} \frac{d^2}{dz^2} + V(z) \right] f(z) = \epsilon f(z), \tag{7}$$

where $m^*(z)$ is the effective mass (its z dependence indicating that m^* is different in different layers) and $f(z)$ is the envelope function.

According to the scheme of Fig. 10, in symmetric DQW

structures of interest in this paper the confinement potential $V(z)$ for the carriers has the following profile:

$$V^h(z)=\begin{cases} 0, & L_b/2<|z|<L_b/2+L_w \\ V_b^h, & |z|\leqslant L_b/2 \\ V_o^h, & L_b/2+L_w<|z|<\infty, \end{cases} \tag{8}$$

$$V^e(z)=\begin{cases} E_g, & L_b/2<|z|<L_b/2+L_w \\ E_g+V_b^e, & |z|\leqslant L_b/2 \\ E_g+V_o^e, & L_b/2+L_w<|z|<\infty, \end{cases} \tag{9}$$

where L_w is the width of each well, L_b is the width of the central barrier, $V_b^{e,h}$ is the central barrier potential for electrons (e) and holes (h), and $V_o^{e,h}$ is the height of the outside barrier for these carriers. Since the potential profile is symmetric, the wave functions of the carriers should have either purely even or purely odd parity in the z direction, their derivatives having alternative parities. Furthermore, the wave functions penetrating the ZnSe barrier regions must decay exponentially with increasing $|z|$. Thus we choose $f(z)\sim e^{-\kappa|z|}$ for the z dependence of the wave function. The Schrödinger equation can be easily solved using the transfer-matrix method[14] when the usual boundary conditions for the wave functions are imposed, i.e.,

$$f(z)/f'(z)=e^{-\kappa z}/(-\kappa e^{-\kappa z})=-1/\kappa, \tag{10}$$

with parameters defined by

$$\frac{2m_i^*(V_i-\epsilon)}{\hbar^2}=\begin{cases} \kappa_i^2, & \text{for } V_i>\epsilon \\ -k_i^2, & \text{for } V_i<\epsilon, \end{cases} \tag{11}$$

where the subscript i refers to electrons and holes, and V_i is given by Eqs. (8) and (9). The dispersion relations for the eigenstates of the DQW's in the energy range $\epsilon<V_o, V_b$ are obtained as follows:

$$\sin(2k_wL_w)\left[\left(\frac{1}{\xi}-\xi\right)\sinh(\kappa_bL_b)+\left(\frac{1}{\eta}-\eta\right)\cosh(\kappa_bL_b)\right]+2\cos(2k_wL_w)\cosh(\kappa_bL_b)$$
$$+\sinh(\kappa_bL_b)\left[\left(\frac{1}{\xi\eta}+\xi\eta\right)\sin^2(k_wL_w)+\left(\frac{\xi}{\eta}+\frac{\eta}{\xi}\right)\cos^2(k_wL_w)\right]=0, \tag{12}$$

with $\xi=k_wm_b^*/\kappa_bm_w^*$ and $\eta=k_wm_o^*/\kappa_om_w^*$. In the region of energy $V_o\geqslant\epsilon\geqslant V_b$ we just need to redefine the variables $\kappa_bL_b\rightarrow ik_bL_b$ and $\xi\rightarrow -ik_wm_b^*/k_bm_w^*$ in the above equation. The eigenenergies are obtained from Eq. (12) for the conduction-band electrons, as well as for the heavy and light holes, by finding ξ and η. Since ξ and η are implicitly functions of the energy ϵ, the eigenstates clearly depend on the barrier potential via relation (11).

In the above formulation we have treated all bands (conduction, heavy hole, light hole, and spin-orbit split-off bands) separately. In a real semiconductor, however, the band structure is much more complex. In the valence band, two bands are degenerate at the band edge, and a third lies nearby, removed from the others by the spin-orbit splitting energy Δ. Furthermore, all the bands interact with each other, and the band structure depends on the strength of such interband interactions, given by

$$P=-\frac{i}{m}\langle S|p_x|X\rangle=-\frac{i}{m}\langle S|p_y|Y\rangle=-\frac{i}{m}\langle S|p_z|Z\rangle, \tag{13}$$

where m is the electron mass, and $|S\rangle$, $|X\rangle$, $|Y\rangle$, and $|Z\rangle$ are the band-edge Bloch functions for the s-like conduction and the three p-like valence bands, respectively. These four bands are doubly degenerate because of spin, and we thus have to consider a total of eight bands together when a magnetic field is involved. An excellent model has been developed for this purpose by Pidgeon and Brown.[15] Based on this model, the Hamiltonian in Eq. (7) becomes an 8×8 matrix in the $\vec{k}\cdot\vec{p}$ approximation,[16] the wave functions having eight components.

The optical transition energy from the nth heavy- or light-hole state to the mth conduction-band state is determined by

$$E_{nm}=E_g^{\text{well}}+E_n+E_m-E_{nm}^B, \tag{14}$$

where E_{nm}^B is the exciton binding energy of the transition. The exciton binding energy in a quantum well will be larger than in the bulk due to quantum confinement. As a consequence, it is also expected to vary with magnetic field[17,18] due to field-induced changes in barrier height. We expect, however, that the magnetic field contribution is a small correction, and our calculations were performed without including this additional variation.

In order to identify the optical transitions, we have to consider the effect of strain due to the lattice mismatch between the layers comprising the DQW. Strain contributes to the splitting between the heavy- and the light-hole levels, in addition to the splitting of these states due to the confinement energy for the different carrier masses. Since wells in the DQW system are under high strain, the strain-induced splitting can be much larger than the splitting due to the mass difference. The influence of strain can be included by adding a strain term H_{st} to the Hamiltonian,[19] given by

$$H_{\text{st}}=C_c\sum_i \epsilon_{ii}-a_v\sum_i \epsilon_{ii}-b_v\sum_i \epsilon_{ii}\left(J_i^2-\frac{1}{3}J^2\right)$$
$$-\frac{d_v}{\sqrt{3}}\sum_{i<j} \epsilon_{ij}\{J_iJ_j\}. \tag{15}$$

Here J is the angular momentum operator for heavy and light holes, C_c is the conduction-band deformation potential con-

stant, a_v is the valence-band hydrostatic deformation potential constant, b_v and d_v are the shear deformation potential constants, and ϵ_{ij} are the components of the strain tensor.

The model that fully describes the electronic states of DQW's in the presence of a magnetic field must include all the contributions discussed above. This results in a Schrödinger equation with a complicated 8×8 matrix form, which cannot be solved analytically. A recently developed numerical technique that has proven extremely useful for dealing with complicated semiconductor heterostructures is the so-called ''finite element method.''[20] This method has facilitated the inclusion of a great number of perturbations[2,21] (such as compressive and tensile strain, modulation doping, and external electric and magnetic fields) in semiconductor heterostructures that lack periodic symmetry. This method, based on the variational principle, allows a systematic approach to improving accuracy by the use of additional finite elements comprising each physical region. It also provides the flexibility to include additional elements, as needed, to represent the variation of the Mn^{2+} concentration at the interfaces. It is thus ideally suited for the analysis of our DQW structures, including the modeling of DMS/non-DMS interface regions in these system.

The parameters involved in this calculation are the energy gap E_g, the spin-orbit splitting Δ of the valence-band, interband interaction matrix elements P, the valence-band Luttinger parameters[22] ($\gamma_1,\gamma_2,\gamma_3$, and κ), the strain parameters (C_c,a_v,b_v, and d_v),[19] the conduction- and valence-band offsets ($V_0^{e,h}$ and $V_b^{e,h}$), and four DMS parameters ($\alpha,\beta,\bar{x}$, and T_0) appearing in Eqs. (2)–(4). The results of numerical calculations using this model will be discussed in the next section.

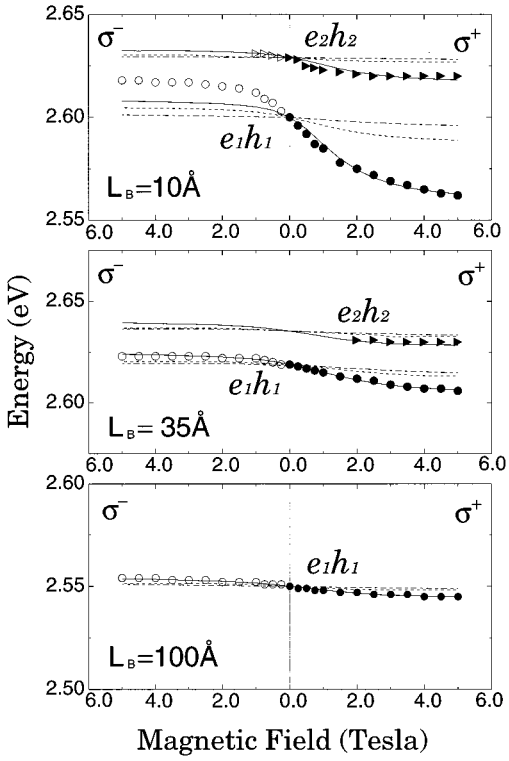

FIG. 11. Results of theoretical calculation for the e_1h_1 and e_2h_2 transition energies for the three DQW's, plotted together with experimental results. The dotted-dashed lines show results obtained without considering interface effects. The dotted lines show results obtained after including diffusion. The solid lines are the ''best fit,'' obtained by introducing intrinsic interface effects, as dicussed in the text.

B. Best fit and discussion

Using the above theoretical model, we calculated the eigenstates for the DQW's. We began with nominal values for the dimensions of the structures, provided by the MBE growers. The Cd and Mn^{2+} concentrations in the respective layers of the DQW were determined from the energy gaps of the corresponding companion $Zn_{1-y}Cd_ySe$ and $Zn_{1-x}Mn_xSe$ epilayers. The strain parameters used in the calculation were taken from Ref. 23, and the band parameters Δ, P, $\gamma_1,\gamma_2,\gamma_3$, and κ from Ref. 2. For band alignment, we assumed that 18% of the band-gap difference between ZnSe and $Zn_{1-y}Cd_ySe$ is accommodated in the valence band.[24] We then optimized the well and barrier thicknesses (within about 10% of the nominal values) by fitting the optical transition energies observed in the absence of magnetic field. Finally, the remaining DMS parameters $\bar{x}$ and T_0 were determined from the Zeeman splitting observed on the companion $Zn_{1-x}Mn_xSe$ epilayer ($\bar{x}=0.040$, $T_0=2.95$ K; see Fig. 5). We then computed the transition energies of the DQW's in the presence of magnetic field, using the parameters in the model described above. The results of the calculations, however, consistently showed much weaker magnetic field dependence of the peak positions than was experimentally observed, and could not fit any of our experimental data. The results of these calculations are shown by the the dotted-dashed lines in Fig. 11. This clearly indicates that the actual variation of the DMS barrier height with magnetic field (i.e., the Zeeman splitting of its band edges) is much stronger than calculated by the model described above. It might appear at first glance that the value of $\bar{x}$ is not known precisely, and the fit could be improved by adjusting this parameter. However, inspection of Fig. 2 indicates that our value of $\bar{x}$ is close to its maximum value. Thus any adjustment in the actual Mn^{2+} concentration x would result in a reduction of $\bar{x}$, and thus of the Zeeman variation of the barrier. To illustrate the disagreement between the model described above and the experiment we note that, to fit the Zeeman splitting observed for the thinnest barrier, we would have to adjust $\bar{x}$ to the value of 0.15, in sharp disagreement with the constraints imposed on this parameter by Fig. 2.

Such drastic differences between the observed data and the calculated behavior therefore indicate that the model used in the calculations must be reexamined. In particular, Fig. 11 suggests that either the Zeeman splitting of the barrier material is much greater than that of the companion epilayer, or that the active barrier region exceeds the dimensions of L_b given in Table I, or both. Both these effects can arise due to the presence of interfaces. In the section below we examine the role of interfaces in determining the Zeeman splitting of a thin DMS layer, and its implications in the context of DQW's.

C. Discussion of DMS/non-DMS interfaces

Recently, enhancements of Zeeman splitting in excess of the value predicted by standard analysis have been observed

in several SQW structures and superlattices[25–31] whose barriers were made from DMS layers ($Cd_{1-x}Mn_xTe$). Two physical mechanisms can be responsible for this behavior: an ''intrinsic'' effect arising from the reduction of the number of antiferromagnetic neighbors of Mn^{2+} ions lying in the interface, and a progressive dilution of the Mn^{2+} concentration across the interface due to interdiffusion (''graded'' interface). The relative importance of these two contributions has been a matter of debate. Gaj *et al.*[28] and Grieshaber *et al.*[31] have proposed a model that takes into account both contributions. These authors conclude that, for a single monolayer of $Cd_{1-x}Mn_xTe$, both effects are comparable in importance. However, they suggest that for an interface between extended DMS and non-DMS regions, the ''extrinsic'' contribution (the grading of the interface due to interdiffusion) is dominant, and is more pronounced for inverted than for normal interfaces. Other authors, on the other hand, attach primary importance to the intrinsic magnetic properties of the near-interface region.[29]

In all structures studied in the above investigations, however, only the tail of the wave function describing the particle in the well interacts with the Mn^{2+} spins in the DMS barrier. In the present case of DQW's, on the other hand, the magnetic layer exists at the center of the structure, so that a much greater fraction of the wave function penetrates the DMS material, making it particularly sensitive to interactions with the magnetic ions within the barrier layer as well as at its interfaces. Clearly, when the DMS barrier separating the wells is thick, the DQW structure effectively becomes two SQW's. Then the magnetic behavior exhibited by the structure will be essentially the same as that of the SQW studied in Refs. 26–28.

We will begin by considering the possibility of diffusion of Mn^{2+} ions into the $Zn_{1-y}Cd_ySe$ wells. This can be taken into account by using an error function profile to represent the diffusion region. If we assume 2 ML as a reasonable diffusion length[27,28] at the interface between wells and the DMS barrier, we obtain a symmetric profile at both sides of the barrier, because the error function has even parity. The simulated potential profile for such symmetric diffusion is schematically shown in Fig. 12(a). Since the diffusion region can be treated as an alloy with a reduced (actual) Mn^{2+} concentration, we can use $\overline{x}$ and T_0 as scale factors in that region, while $\overline{x}$ and T_0 in the barrier are kept the same as in the companion epilayer. However, in bulk DMS's the maximum effective manganese concentration is $\overline{x} \approx 0.04$ (see Fig. 2), corresponding to $x \approx 0.15$, which is close to the Mn^{2+} concentration in the DMS barriers of our DQW's. Thus we can vary $\overline{x}$ in the diffusion region only within the range $0 \leqslant \overline{x} \leqslant 0.04$. The results of the calculation, including the diffusion effect, did not improve the fit significantly. The best results obtained in this way are shown in Fig. 11 as dotted lines. The figure clearly shows that the thinner the barrier, the worse the fit.

It was pointed out[28] that interface diffusion of Mn^{2+} ions that occurs during MBE growth may be different for non-DMS material grown on DMS (so called ''inverted'' interface), and for DMS material grown on non-DMS (''normal'' interface), due to lattice mismatch between the two materials. This would result in an asymmetric interface profile, described by an exponential function at either side of the DMS barrier in a DQW. We can simulate this asymmetric effect by assuming different diffusion lengths for the two sides of the barrier, as shown in Fig. 12(b), and different effective Mn^{2+} concentrations on either side. However, for any configuration that we attempted, the calculation still showed consistently much smaller Zeeman splitting than was experimentally observed. (It is worth noting that the flexibility of the finite element method[20] discussed in Sec. V A makes the simulations described above particularly straightforward.)

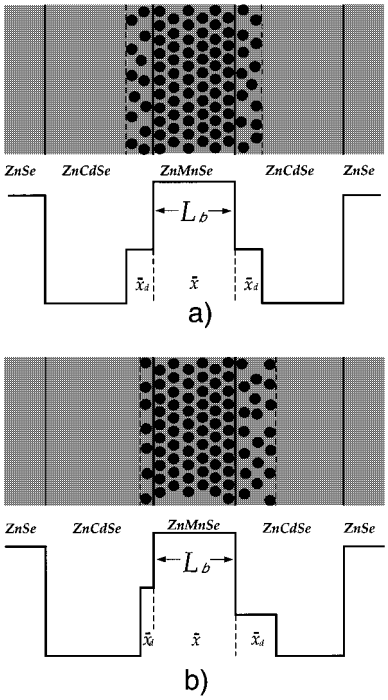

FIG. 12. A qualitative diffusion picture for Mn ions at the $Zn_{1-x}Cd_xSe/Zn_{1-x}Mn_xSe$ interface in a DQW, together with the corresponding potential profile simulation. Here the black dots indicate manganese ions which diffuse into the $Zn_{1-x}Cd_xSe$ wells; and $\overline{x}$ and $\overline{x_d}$ are the effective manganese concentrations for the DMS barrier material and for the diffusion region, respectively. We use the same $\overline{x}$ as in the companion epilayer, and vary $\overline{x_d}$ for fitting experimental data. Upper and lower panels depict symmetric and antisymmetric diffusion, as discussed in the text.

One can of course obtain larger Zeeman splittings of the absorption lines if Mn^{2+} ions are assumed to diffuse deep into the wells (diffusion length much larger than two or three atomic layers). Reasoning in this way, we can estimate the diffusion length required to obtain the observed shift of the e_1h_1 line by comparing the Zeeman shift observed for the $Zn_{1-x}Mn_xSe$ epilayer in Fig. 5, and that of the e_1h_1 transition for the σ^+ polarization in the DQW with a 10-Å barrier, Fig. 4. Since the e_1h_1 transition shift reaches about 80% of the epilayer Zeeman shift, the Mn^{2+} ions should diffuse about 80% of the well width in the DQW. This leads to a diffusion length of about 12 ML, which is unreasonably large (over 30 Å), and is in drastic disagreement with studies of diffusion by others, most of which favor diffusion lengths not greater than 3 ML. Such large diffusion lengths would, furthermore, result in the shift observed for e_1h_1 and e_2h_2 being comparable in *all* three samples, which is clearly contrary to observation. We must therefore look for another ex-

TABLE II. Best fit parameters for the 2-ML interface region.

Sample	Barrier thickness	$\overline{x}$	T_0
1	10 Å	0.12	1.2 K
2	35 Å	0.06	1.5 K
3	100 Å	0.047	1.5 K
Epilayer	1 μm	0.04	2.95 K

planation, and we now examine the intrinsic magnetism of an abrupt DMS/non-DMS interface in this context.

It is well known that the nearest-neighbor spin-spin exchange interaction between Mn^{2+} ions is antiferromagnetic in bulk Mn-based DMS's. As a consequence, for example, antiferromagnetically coupled spin pairs do not contribute to the average spin $\langle S_z \rangle$ of $Zn_{1-x}Mn_xSe$. Now in the case of an abrupt DMS/non-DMS interface, magnetic ions in the interface plane will in general have a different number of magnetic neighbors than they would within a bulk crystal of the same composition as the DMS layer. For instance, a Mn^{2+} ion within a face-centered cubic lattice (i.e., inside a *bulk* alloy) has 12 nearest-neighbor cation sites, any of which could be occupied by another Mn^{2+} ion; whereas a Mn^{2+} ion at a DMS/non-DMS interface has only 8 nearest-neighbor cation sites that could be occupied by a Mn^{2+} ion. Hence the possibility for finding antiferromagnetically paired ions is reduced at the interface, leading to a larger $\langle S_z \rangle$, and larger magnetization. Such *enhancement of paramagnetism*[8,32] was calculated for the specific case of the 2 ML adjacent to the interface, by considering the statistical distribution of nearest neighbors. When this is expressed in terms of effective Mn^{2+} concentration $\overline{x}$, the enhancement becomes appreciable for concentrations $x \geqslant 0.1$, as shown by the dotted line in Fig. 2. Since the actual Mn^{2+} concentration x of the DMS barriers in our DQW's is in all cases larger than $x=0.1$, this intrinsic interface effect must contribute to the enhancement of the Zeeman splitting exhibited by the barriers in our DQW's.

Invoking a similar approach, we model the barriers of the DQW's as previously, by introducing a 2-ML interface region [as shown in Fig. 12(a)], and we use $\overline{x}$ and T_0 as fitting parameters for this 2-ML region, but this time without imposing limits on their values, in order to simulate such enhanced paramagnetism at the interface. In this calculation we keep $\overline{x}=0.04$ and $T_0=2.95$ K as constant in the original barrier [i.e., in the region L_b in Fig. 12(a)]. With this admittedly rough simulation, we carried out numerical calculations to best fit the energies of the optical transitions observed in the presence of the magnetic field. The values of $\overline{x}$ and T_0 for the 2-ML interface region that gave the best fits to the data are presented in Table II. The results of calculations carried out using these parameters are shown in Fig. 11 as solid lines. As seen from Table II and Fig. 11, the results of this calculation gave a good fit to the data observed on DQW's with the thickest barrier (100 Å) when the effective manganese concentration in the interface region was assumed to be $\overline{x}=0.047$. This is in good agreement with the simulation results of effective manganese concentration obtained by others for DMS/non-DMS interfaces, cited above.[8] However, to fit the data observed on DQW's with thinner barriers, it was necessary to increase the effective concentration of manganese significantly beyond 0.047. For example, for the DQW with 35 Å, we need $\overline{x}=0.06$; and for the DQW with a 10 Å barrier we had to use a value of $\overline{x}=0.12$, three times as large as $\overline{x}$ for the ''companion'' epilayer (and three times as large as the maximum value allowed for this parameter in continuous DMS media). Note, however, that this value is very close to $\overline{x}=0.10$, obtained by Harrison *et al.*[32] in their simulation of a single $Cd_{1-x}Mn_xTe$ monolayer for $x=0.20$. The value of $\overline{x}$ used in obtaining the best fit is plotted as a function of inverse barrier thickness in Fig. 13, to demonstrate the progression of $\overline{x}$ with increasing interface-to-volume ratio of the respective barriers. Table II also indicates another potentially important trend: the effective temperature T_0, which reflects a residual antiferromagnetic interaction between unpaired ''loose'' spins, clearly decreases with decreasing barrier thickness. This reduction of T_0 for spins near the interface demonstrates that those Mn^{2+} spins can more easily be aligned by the magnetic field, and thus more effectively contribute to the total average spin of the system.

The large effective Mn^{2+} concentration $\overline{x}$ required to fit the DQW data gives us important insights into the magnetic properties of thin DMS barriers themselves. This may be expected from the argument that, if the Mn^{2+} ions at the interface make a larger contribution to the total average spin per ion than those in the bulk, clearly the relative number of such interface ions increases as the barrier becomes thinner,

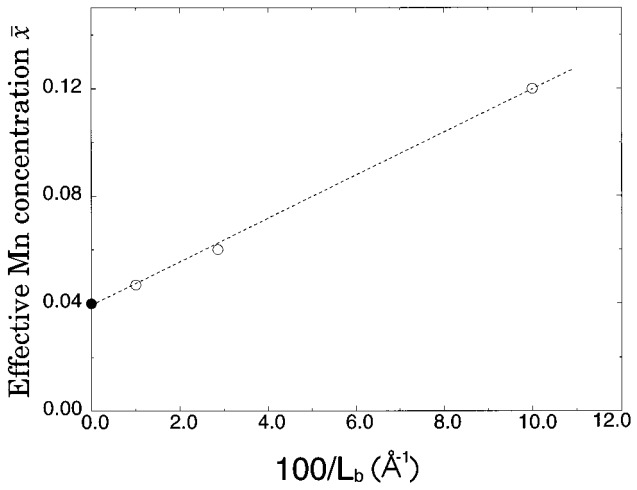

FIG. 13. Effective manganese concentration of the interface region in DQW's, required to give best fit to the observed transitions energies, plotted as a function of inverse DMS barrier thickness. The three samples with different DMS barrier thicknesses show a surprisingly linear dependence of $\overline{x}$ on L_b^{-1}. The black dot at $\overline{x}=0.04$ indicates the effective manganese concentration of the companion epilayer.

i.e., as its interface-to-volume ratio increases. In the limit as the DMS layer approaches an atomic monolayer (i.e., as it becomes ideally 2D), magnetic ions have only four nearest-neighbor sites that could be occupied by other magnetic ions, three times less than in the bulk. Thus the thinner the layer, the larger will be the effective manganese concentration $\bar{x}$ associated with any given x. The systematic increase of the effective manganese concentration needed to fit the data with decreasing barrier thickness (see Table II and Fig. 13) would thus indeed be expected (at least qualitatively) as the DMS layer approaches the 2D limit.

VI. CONCLUSIONS

We have investigated a set of DQW's coupled by DMS barriers, with different barrier thicknesses. As would be expected, we observed the interwell coupling to be strongest in the sample with the thinnest barrier. Using a DMS layer as the barrier provided the opportunity to vary the interwell coupling continuously in any one sample by varying an applied magnetic field. This magnetically induced variation of the coupling clearly manifested itself through the *energy separation* between interband transitions from the two lowest-lying symmetric and antisymmetric states. Furthermore, this behavior was also accompanied by a striking variation of the intensity of these two transitions as the coupling was changing. Specifically, as the e_1h_1 transition (that involving symmetric states) became weaker, the e_2h_2 transition became stronger, in such a way that the integrated intensity for both remained constant. This behavior was not *a priori* expected, but was consistently present for all samples and at all temperatures investigated.

The observed variation of interwell coupling with the magnetic field was consistently much larger than expected on the basis of the standard theory. This in turn indicates that standard analysis underestimates the Zeeman splitting of band edges in thin DMS barrier layers. Our analysis also shows that the observed enhancement of Zeeman splitting cannot be explained exclusively by diffusion of Mn^{2+} ions in the interface region of the DMS barrier. By considering both diffusion and the intrinsic reduction of antiferromagnetic pairing at the interfaces between DMS and non-DMS materials, we were able to discuss quantitatively the behavior of the DQW with the thickest barrier (100 Å). In the DQW's with thinner barriers, however, a discrepancy between the experiments and theoretical calculations (including both diffusion and intrinsic effects) arose, and we needed to increase the effective manganese concentration of the interface region significantly to fit the experimental data. The required increase clearly varied inversely with barrier thickness L_b. This behavior is so systematic that we are tempted to attribute the enhanced Zeeman splitting primarily to dimensional effects (interface-to-volume ratio) as the DMS barrier layer becomes ultrathin. This result is in disagreement with the calculation of Grieshaber *et al.*,[31] which suggest that, for a single monolayer, the contributions of the intrinsic effect and diffusion are comparable. It should be emphasized that the DQW structure with a DMS barrier provides an ideal structure for the study of such enhanced interface paramagnetism, because the wave function of the symmetric eigenstates in this structure is centered *at* the interwell barrier. The system is thus much more sensitive to the magnetic behavior of the DMS/non-DMS interfaces that nonmagnetic SQW's with magnetic barriers, where the interface is ''felt'' only by the tail region of the wave function.

ACKNOWLEDGMENTS

We express our thanks to S.H. Xin and U. Bindley for the preparation of the excellent DQW specimens, and to G. Yang for continuing interest and stimulating discussions. We also wish to thank Quantum Semiconductor Algorithms for the use of their finite element software. This work was supported by the National Science Foundation Grant No. DMR 9208400.

[1] J. K. Furdyna, J. Appl. Phys. **64**, R29 (1988).
[2] See, for example, N. Dai, L. R. Ram-Mohan, H. Luo, G. L. Yang, F.C. Zhang, M. Dobrowolska, and J. K. Furdyna, Phys. Rev. B **50**, 18153 (1994); also J. K. Furdyna, Solid State Electron. **37**, 1065 (1994).
[3] R. Dingle, A. C. Gossard, and W. Wiegmann, Phys. Rev. Lett. **34,** 1327 (1975).
[4] H. Asai and K. Oe, J. Appl. Phys. **54**, 2052 (1983).
[5] J. F. Smyth, D. D. Awschalom, N. Samarth, H. Luo, and J. K. Furdyna, Phys. Rev. B **46,** 4340 (1992).
[6] J. A. Gaj, in *Diluted Magnetic Semiconductors,* edited by J. K. Furdyna and J. Kossut, Semiconductors and Semimetals (Academic, Boston, 1988), Vol. 25, Chap. 7.
[7] J. A. Gaj, R. Planel, and G. Fishman, Solid State Commun. **29**, 435 (1979).
[8] J. M. Fatah, T. Piorek, P. Harrison, T. Stirner, and W. E. Hagston, Phys. Rev. B **49,** 10 341 (1994).
[9] A. Ohki, K. Ando, and S. Zembutsu, J. Electron. Mater. **22,** 529 (1993).
[10] M. Sugawara, J. Appl. Phys. **71**, 277 (1992).
[11] G. Bastard, Phys. Rev. B **24**, 5693 (1981).
[12] G. Bastard, Phys. Rev. B **25**, 7584 (1982).
[13] J. M. Luttinger and W. Kohn, Phys. Rev. **97**, 869 (1955).
[14] L. R. Ram-Mohan, K. H. Yoo, and R. L. Aggarwal, Phys. Rev. B **38,** 6151 (1988).
[15] C. R. Pidgeon and R. N. Brown, Phys. Rev. **146**, 575 (1966).
[16] E. O. Kane, J. Phys. Chem. Solids **1**, 294 (1973).
[17] T. Kamizato and M. Matsuura, Phys. Rev. B **40**, 8378 (1989).
[18] J. Chen and K. K. Bajaj, Phys. Rev. B **46**, 15 208 (1992).
[19] G. L. Bir and G. E. Pikus, *Symmetry and Strain-Induced Effects in Semiconductors* (Wiley, New York, 1972).
[20] L. R. Ram-Mohan, S. Saigal, D. Dossa, and J. Shertzer, Comput. Phys. **4,** 50 (1990).
[21] S. W. Short, S. Xin, A. Yin, H. Lou, M. Dobrowolska, and J. K. Furdyna, J. Electron. Mater. **25**, 253 (1996).
[22] J. M. Luttinger, Phys. Rev. **102**, 1030 (1956).
[23] B. Rockwell, H. R. Chandrasekhar, M. Chandrasekhar, A. K. Ramdas, M. Kobayashi, and R. L. Gunshor, Phys. Rev. B **44**, 11 307 (1991).

[24] T. Nakayama, Jpn. J. Appl. Phys. **33**, L211 (1994).
[25] A. Wasiela, Y. Merle d'Aubigné, J. E. Nicholls, D. E. Ashenford, and B. Lunn, Solid State Commun. **76**, 263 (1990).
[26] R. Meyer, M. Hirsch, G. Schaack, A. Wagg, and R.-N. Bicknell-Tassius, Superlattices Microstruct. **9**, 165 (1991).
[27] S. R. Jackson, J. E. Nicholls, W. E. Hagston, P. Harrison, T. Stirner, and J. H. C. Hogg, Phys. Rev. B **50**, 5392 (1994).
[28] J. A. Gaj, W. Grieshaber, C. Bodin-Deshayes, J. Cibert, Y. Merle d'Aubigné, and A. Wasiela, Phys. Rev. B **50**, 5512 (1994).
[29] W. J. Ossau and B. Kuhn-Heinrich, Physica B **184**, 422 (1993).
[30] D. R. Yakovlev, Adv. Solid State Phys. **32**, 251 (1992).
[31] W. Grieshaber, A. Haury, J. Ciber, Y. Merle d'Aubigne, A. Wasiela, and J. A. Gaj, Phys. Rev. B **53**, 4891 (1996).
[32] P. Harrison, J. M. Fatah, T. Stirner, and W. E. Hagston, J. Appl. Phys. **79**, 1683 (1996).